Periodic orbits and the homoclinic tangle in atom-surface chaotic scattering

R. Guantes and F. Borondo
Departamento de Química, C-IX, Universidad Autónoma de Madrid, Cantoblanco, 28049 Madrid, Spain

S. Miret-Artés
Max-Planck-Institut für Strömungsforschung, Bunsenstraβe 10, D-37073 Göttingen, Germany
(Received 20 January 1997; revised manuscript received 20 March 1997)

In this paper the phase-space structure of a realistic chaotic scattering system, namely, the collisions of He atoms off Cu surfaces with different degrees of corrugation, is investigated. We demonstrate that the homoclinic tangle generated by a principal unstable periodic orbit, which corresponds to the unperturbed motion of the He atom traveling parallel to the surface in the asymptotic region, determines the entire scattering dynamics of the system. The fractal properties and some physical invariant features of the system can be understood using suitable Poincaré surfaces of section. Moreover, in this paper we also analyze in detail the periodic orbit structure in the interaction region, and show how the homoclinic chaotic trajectories can be organized in a similar fashion to the well-known Farey tree organization for resonances. The consequences of this analogy for the different scaling laws observed in chaotic scattering problems are discussed. [S1063-651X(97)13107-5]

PACS number(s): 05.45.+b, 79.20.Rf

I. INTRODUCTION

Many processes of chemical and physical interest (gas phase chemical reactions, adsorption and diffusion on surfaces, etc.) can be adequately treated just at the classical level [1,2], and here the understanding of the Hamiltonian dynamics and phase space has been determinant in the development of classical and semiclassical theories [5,6]. These theories are often an easier and accurate enough alternative route to more complicated quantum calculations, and many times are based on the assumption that the underlying dynamics are chaotic [3,4]. Although the existence of chaotic scattering in some simple models of chemical reactions and diffraction of atoms from surfaces was observed two decades ago [7,8] (and not always properly identified), only quite recently has it begun to be intensively studied and characterized from the mathematical point of view. Many studies in chaotic scattering have been done with simple models [9], mainly area-preserving maps and hard-wall potentials, although some molecular systems have also been considered [10–12]. The distinctive feature of scattering systems is the infinite volume of the phase space at a given energy due to the existence of an asymptotic region where the interaction potential can be neglected. The observables are calculated in the final asymptotic region where the dynamics is trivially integrable, although they obviously depend on the intricacies of the potential in the interaction region. In this sense a knowledge of the bound dynamics within the interaction region can help to clarify the long-time behavior of the chaotic dynamics (the existence of the set of singularities of the scattering functions that connect incoming to outgoing asymptotic regions).

The present contribution was motivated by some recent results of the authors [12] in the numerical investigation of the classical dynamics of a realistic model for the scattering of He atoms from Cu surfaces. There, as in previous works on other physical scattering systems such as atom-diatom collisions, encounters of artificial satellites, dynamics of vortices, scattering off a magnetic dipole, etc. [10,13,14], a fractal structure was observed in the plots of a scattering function (final scattering angle or time delays) corresponding to an underlying Cantor set of singularities. The main scaling laws of this Cantor set were numerically found and applied in a semiclassical study of diffraction intensities [12].

The self-similarity and other fractal features of the scattering function plots are a direct consequence of the partition of the phase space into an invariant fractal tiling [11(c)] which organizes the scattering dynamics in a very systematic way. Realistic models for atom-molecule or atom-surface interactions imply the use of soft potentials or potentials attractive for large distances and repulsive for short distances. In our case, as in other soft interacting systems with periodicities in the potential [11,15,16], the asymptotic motion is an unstable periodic orbit whose stable and unstable manifolds determine the entire scattering dynamics of the system. In analogy to previous work in one-dimensional maps and atom-molecule collisions [19,11] hereafter we will call this the principal unstable periodic orbit (PUPO). In this paper we show, for the scattering of He atoms off corrugated Cu surfaces, how the use of the Poincaré surface of section (SOS) of the homoclinic tangle originated by the PUPO at a given energy provides a coherent picture of the scattering dynamics and its interaction with the classical objects present into the bounded region. Moreover, the close relation existing between chaotic scattering trajectories and the principal periodic orbits (PO's) of the system will be also analyzed in detail, establishing a connection between the Farey tree organization of PO's and the symbolic dynamics for chaotic scattering trajectories. In the chaotic regime, the properties of the scattering functions (fractal dimension of the invariant set of singularities, scaling laws, escape rates of the chaotic trajectories, etc.) depend on the value of some parameters of the Hamiltonian. The natural choice for such parameters in conservative Hamiltonian systems is the total

TABLE I. Potential energy surface for the scattering of He from Cu surfaces at 21 meV [17].

Potential energy: $V(x,z)=V_M(z)+V_C(x,z)$
Morse potential: $V_M(z)=D(1-e^{-\alpha z})^2$
$D=6.35$ meV, $\alpha=1.05$ Å^{-1}
Coupling potential: $V_C(x,z)=V_z(z)V_x(x)$
$V_z(z)=D\exp(-2\alpha z)$
$V_x(x)=\sum_n\left[r_n\cos\frac{2n\pi x}{a}+s_n\sin\frac{2n\pi x}{a}\right]$

Fourier coefficients for Cu(110):
$r_1=0.03$, $s_1=0.0$
$r_2=0.0004$, $s_2=0.0$
Unit cell length for Cu(110): $a=3.6$ Å

Fourier coefficients for Cu(117):
$r_1=0.1828$, $s_1=-0.0836$
$r_2=0.0593$, $s_2=0.0157$
$r_3=0.0116$, $s_3=0.0002$
$r_4=0.0017$, $s_4=0.0010$
Unit cell length for Cu(117): $a=9.12$ Å

energy, and the bifurcations of the main principal families of PO's with the energy will be considered. Also, the influence of the corrugation of the surface will be studied by analyzing two different crystallographic faces.

The organization of the paper is as follows. In Sec. II we give a brief account of the model employed, which has been described elsewhere [12], and of the main conclusions obtained in the numerical investigation of the final scattering angles vs initial impact parameter plots. In Sec. III, the geometry imposed in the phase space by the homoclinic tangle is discussed, and its relation to the results in the final angle vs impact parameter plots described. Section IV is devoted to a study of the bounded region of the system, presenting an analysis of the main PO's and their evolution with energy. The interrelation between the bounded and the scattering dynamics is considered in Sec. V. The paper is concluded by summarizing our conclusions in Sec. VI.

II. MODEL SYSTEM AND TRAJECTORY CALCULATIONS

The problem we have chosen to study is the scattering of ^{4}He atoms off Cu surfaces with different degrees of corrugation. In particular, elastic collisions with Cu(110) and Cu(117) will be considered. The system can be modeled with a two degrees of freedom Hamiltonian

$$H(P_x,P_z,x,z)=\frac{P_x^2+P_z^2}{2m}+V(x,z), \tag{1}$$

where x and z are coordinates parallel and perpendicular to the surface, respectively, and $V(x,z)$ is a corrugated Morse potential, whose parameters have been taken from the literature [17] and are presented in Table I. It is interesting to note at this point that the corrugation for Cu(110) is just a sum of cosine functions, so that the potential is symmetric with respect to the $x=0,a$ and $x=a/2$ planes (a being the unit cell length). The more corrugated Cu(117) function does not have this symmetry.

Classical trajectories are propagated starting from the following initial conditions

$$\begin{aligned} z_0&=z_{\max}\\ x_0&=-z_{\max}\tan\theta_i+ba\\ P_{z_0}&=-\sqrt{2mE}\cos\theta_i\\ P_{x_0}&=\sqrt{2mE}\sin\theta_i, \end{aligned} \tag{2}$$

where $z_{\max}$ represents a value of z sufficiently large so that the interaction potential can be neglected, b is the normalized impact parameter ($0\leqslant b\leqslant 1$), E the collision energy, and θ_i the initial incident angle. This angle θ_i initially determines the partition of the total energy and momentum between the two modes.

In previous work [12] many trajectories were calculated and analyzed. In those papers our attention focused on the transition to chaos, considering the scattering at different values of the incident angle θ_i at a fixed value of the energy. The onset of chaos was identified in the classical deflection function (final scattering angle θ_f) vs impact parameter plots when one of the rainbow angles (maxima or minima of the classical deflection function) reaches a value of 90° [12(a)]. At these points, what happens is that when the He particle hits the inner wall of the potential (low values of z), enough momentum (or translational energy) is transferred from the perpendicular to the parallel modes, and the trajectory becomes trapped inside the potential well existing along the perpendicular mode. Afterwards, the He particle begins its motion, repeatedly bouncing with the Cu surface, until enough perpendicular momentum is regained that it can leave the surface. In those flights the particle travels a distance corresponding to many cell units, loosing memory of the initial conditions. The θ_f-b plots then consist of a smooth, well-behaved part corresponding to direct scattering, and a very ill-behaved region of trapped trajectories called the chattering region (see, for example, Fig. 1 below). The chattering region consists in turn of a series of smooth subdomains or *icicles* [10(c)], separated by regions of more complicated behavior containing an infinite number of singularities [see Fig. 1(c)]. When these chaotic regions are expanded they again show the same structure at finer and finer scales. The whole structure is then a (multi)fractal [18]. Moreover, the icicles observed in the chattering regions of the θ_f-b plots are organized in a hierarchical way. All trajectories associated with a given icicle are alike, and can be characterized by the number of bounces with the surface and the number of units cells traveled between consecutive bounces. Then a symbolic labeling can be used to classify them. An extra symbol is required in this case, namely, ''+'' or ''−,'' indicating if a given icicle is situated to the right or left of the central icicle, which corresponds to the icicle with a minimum number of unit cells traveled. One

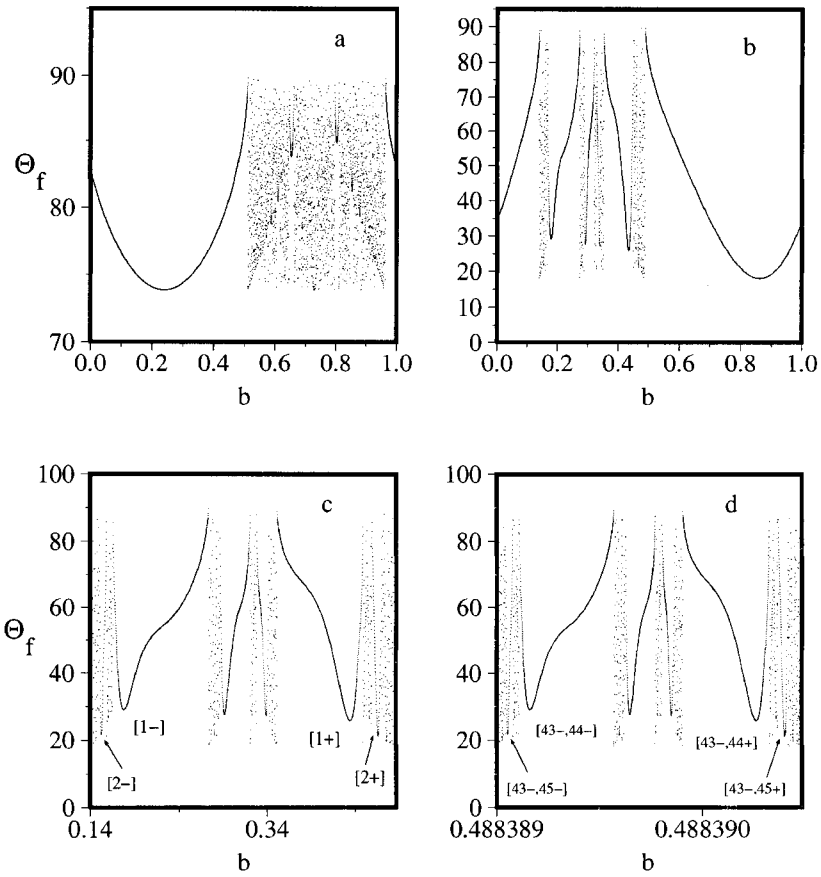

FIG. 1. Final scattering angle θ_f (in degrees) vs impact parameter b for the scattering of ^{4}He atoms off (a) Cu(110) surfaces, and (b) Cu(117) surfaces, at a total energy of $E=21$ meV and an incident angle $\theta_i=90°$. (c) Expansion of the chattering region appearing in part (b). (d) Expansion of the gap between icicles $[42^-]$ and $[43^-]$ of part (c).

possible unique labeling scheme constructed along this line was given in Ref. [12](a), and will be used throughout the paper.

In Figs. 1(a) and 1(b) the θ_f-b plots for the Cu(110) and Cu(117) surfaces at a total energy of 21 meV and $\theta_i=90°$ are presented. The central icicles of the chattering regions in both figures correspond to trapped trajectories bouncing twice on the surface and traveling, respectively, eight and one unit cells in the jump. The number of traveled unit cells increases by one as we move to the next icicle either to the right or to the left in the chattering region. In Fig. 1(c) we present, expanded, the chattering region corresponding to Cu(117) [Fig. 1(b)]. In it, all features described are readily observed. Let us consider now what happens in the gaps between icicles of this first generation. For example, an expansion of the region between icicles $[42^-]$ and $[43^-]$ is presented in Fig. 1(d). In it one observes the icicles associated with the trapped trajectories $[43^-,n]$ for Cu(117). The corresponding trajectories bounce three times with the surface, traveling 43 unit cells in the first jump, and n (beginning from $n=1$ for the two central icicles) in the second. This pattern, which repeats hierarchically on all scales, will play an important role in the rest of the discussions in the paper. It allows one to label each icicle by m signed integers, the first $m-1$ identifying the generation to which the icicle belongs, and the last one identifying the position of the icicle within its own generation. As we will discuss later, the fractal structure of the chattering region can be considered asymptotically [sufficiently far apart from the center of the chattering region, since we see in Figs. 1(c) and 1(d) that the invariant shape of the pattern is achieved for gaps close to the edges] a two-scale fractal. We consider that there is one intragenerational scaling factor α mapping a given icicle or gap of one generation of the fractal into an icicle or gap inside the same generation, and an intergenerational scaling factor β which transforms an invariant pattern of one generation into a pattern of another generation. For Cu(117), both scaling factors were numerically found to be $\alpha=0.98$ and $\beta=0.000\,35$ [12(c)]. Moreover, these values are *independent* of the incidence angle, and we also found that the invariant pattern of Figs. 1(c) and 1(d) are identical to the whole chattering region obtained at grazing angles (approximately 90°). The same conclusion is true for other scattering functions such as delay times or other fractal properties (fractal dimension or escape rate). In Sec. III we explain this invariance with respect to the initial angle θ_i by means of the SOS of the phase space.

III. HOMOCLINIC TANGLE AND FRACTAL INVARIANT TILING

As was mentioned in Sec. I, the whole dynamics of the He-Cu scattering process can be presented in a rather compact way by considering the homoclinic tangle [19] formed in phase space by the stable and unstable manifolds emanating from the PUPO. According to what was discussed about

the origin of the onset of chaos in the preceding section, the PUPO in our system corresponds to a trajectory in which the He atom travels parallel to the Cu surface at an infinite separation of it ($z > z_{max}$, $P_x \geq 0$). Since the potential function [17] is periodic along x, the dynamics of the trajectories can be followed quite conveniently by using a (z,P_z) Poincaré surface of section (SOS) taking $x = x_0 + na$ ($n = 0,1, \ldots, \infty$) as the sectioning plane. Obviously, $x_0 = 0, a$ or $x_0 = a/2$ are good choices to obtain a dynamically significant SOS, especially in the more symmetric Cu(110) case (see Fourier coefficients in Table I).

The corresponding results for an energy of 21 meV are shown in Fig. 2 for both corrugations, Cu(110) and Cu(117), considered in this paper and the SOS placed at $x_0 = 0$. Notice in passing that Fig. 1(a) corresponds to the θ_f-b plot of the homoclinic tangle unstable branch (propagation forward in time). When examined the two plots presented in Fig. 2 are very different. At this energy, the scattering for Cu(110) [Fig. 2(a)] exhibits a mixed dynamics, that is, chaotic trajectories coexist with regular *KAM* islands, which are organized in this case around the stable periodic perpendicular motion (x constant). This corresponds to what is called in the literature a nonhyperbolic regime [20], which is characterized by presenting an algebraic survival probability or exit time of the trapped trajectories [21]. On the other hand, for the Cu(117) surface the manifolds appear much more deformed, suggesting a more irregular dynamics. The area enclosed by the oscillations (lobes and turnstiles [19]) is larger, which indicates that the transport from the scattering to the trapped [23] region is larger. Also, no visible traces of regularity are observed in this region. As we will see in Sec. IV, the central stable PO has become unstable. This suggest that the dynamics should be hyperbolic. Proving the hyperbolicity of a dynamical system is a very difficult task for other than simple analytical maps. There are, however, several numerical criteria to distinguish between hyperbolic and nonhyperbolic regimes. The hyperbolic regime is in general characterized by exponential escape rates of the trapped trajectories [21], and also by a Gaussian distribution in the Lyapunov exponents spectra [24]. In our case we will show that the main PO is highly unstable, and that no further bifurcations for higher energies take place; this implies that the last homoclinic tangency [19] has taken place, and that we are in the hyperbolic or fully developed chaotic regime [9]. Here it is necessary to point out that sometimes power-law escape rates have also been found in hyperbolic systems [20(a),20(b)]. This happens in our model too. Since at long distances the Morse potential is the dominant part of the interaction, and this potential tends exponentially slowly to the top of the ridge, D, one can see that the PUPO is a parabolic point of the Poincaré map. Consequently, nearby orbits diverge only linearly with time and escape rates present a power law behavior [22].

There is another aspect of Fig. 2 worth commenting upon. The homoclinic tangle partitions phase space into two unconnected regions: one external, where only direct scattering take place; and another internal, corresponding to bounded dynamics, where trajectories are trapped for some time before they leave the surface. Due to the symmetries in the potential, this curve is symmetric upon reflection through the $P_z = 0$ plane for Cu(110), and nonsymmetric for Cu(117).

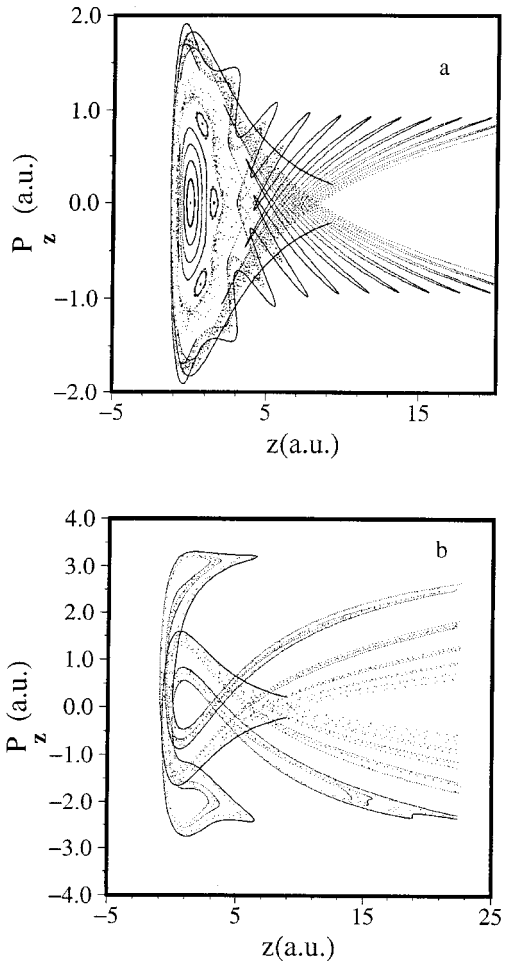

FIG. 2. Homoclinic tangle corresponding to the principle unstable periodic orbit (PUPO) at $E = 21$ meV for the scattering off (a) Cu(110) and (b) Cu(117) surfaces.

In Fig. 3 we plot the pseudoseparatrix of the homoclinic tangle for the Cu(110) surface. It was obtained by propagating only the initial conditions corresponding to the direct collisions part of Fig. 1(a). According to the transport theory of Hamiltonian systems [19], every trajectory initiated inside the pseudoseparatrix will enter the interaction region through the entrance turnstile, and will remain trapped in it for some time before leaving it through the exit turnstile [see Fig. 3(a)]. In a recent paper, Tiyapan and Jaffé [11(c)] showed how every group of complex forming trajectories gives rise to a sequence of tiles inside the interaction region, in such a way that the whole area can be covered hierarchically with them. Moreover, the characteristics of this sequence of tiles is related to the characteristics of the trajectories. Thus, the fractal character of the θ_f-b plots is a mere reflection of the fractal *invariant* tiling of the interaction region. Let us consider, for example, the two central icicles of the chattering region for Cu(110), labeled $[8^{\pm}]$. By propagating them forward and backwards in time the pattern shown with thick lines in Fig. 3(b) is obtained. To help following the dynamics, we have numbered in the figure the consecutive iterations corresponding to the propagation forward. This propagation forward gives the two segments of each tile confined to the unstable manifold (one segment per icicle), while the propagation backward renders the two segments confined to

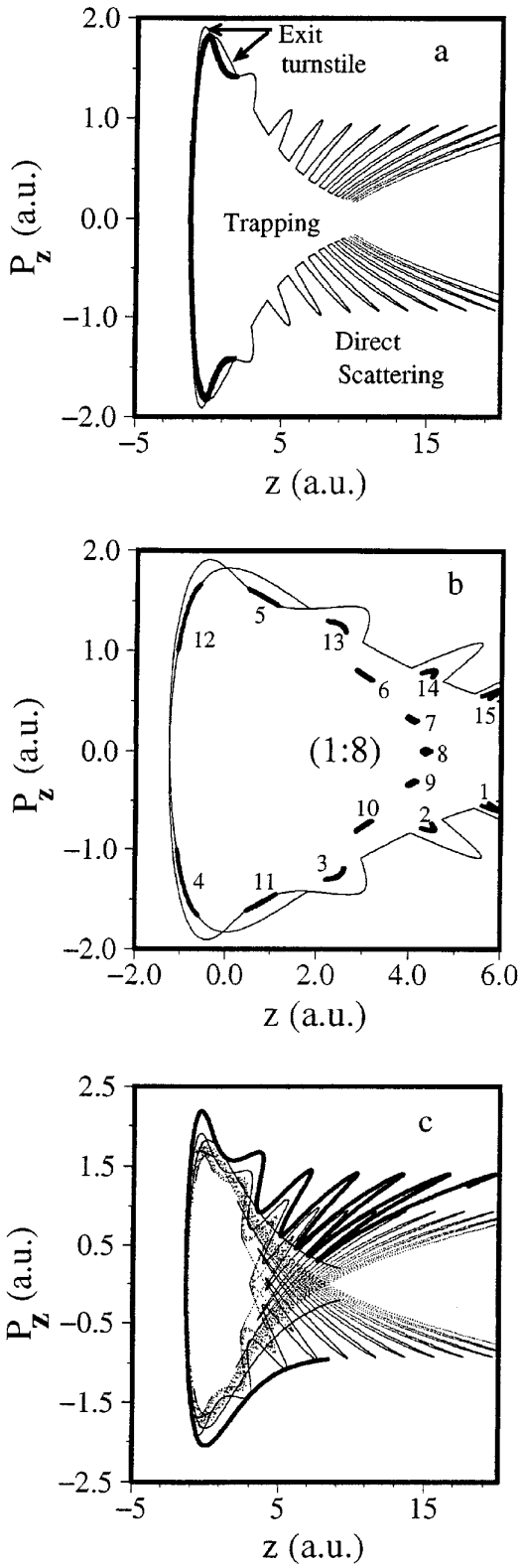

FIG. 3. (a) Pseudoseparatrix between direct and chaotic scattering for the He-Cu(110) surface collisions at $E=21$ meV. The inner part of the turnstiles have been marked with thick lines. (b) Family of tiles (1:8) corresponding to the $[8^{\pm}]$ icicles. (c) Homoclinic tangle associated with the He-Cu(110) scattering principle unstable periodic orbit (dots) at $E=21$ meV, and unstable manifold (thick line) for $\theta_i=74°$ at the same energy. Notice that this manifold corresponds to the onset of chaos in this scattering problem.

the stable branch. The intersection points are the homoclinic trajectories belonging both to the stable and unstable branches, which are asymptotic in the infinite past and future to the PUPO. In our case, the homoclinic orbits correspond to the leftmost and rightmost points of each icicle; for them $\theta_f=90°$, and therefore constitute the chaotic component of the dynamics or the invariant Cantor set [18] of singularities present in the θ_f-b plots. This set is of measure zero and countable.

In analogy to the symbolic labeling of the icicles described in Sec. II, a labeling scheme for the tiles can be devised. Any given trapped trajectory will visit as many tiles inside the interaction region as the total number of unit cells traveled between the first and last bounces (remember that we have placed our SOS at intervals of periodicity a). Consequently, each different type of trajectory or icicle will give rise to a family of tiles characterized by two numbers $(m:n)$, m being the number of times the tiles cross the $P_z=0$ line (equivalent to the generation or number of bounces of the trapped trajectory), and n the total number of tiles inside the interaction region (total number of unit cells jumped). Notice that there is not a one-to-one correspondence between icicles and families of tiles, since in general there will be several icicles (at least two, one from the right part of the fractal and the other from the left) originating from the same family. However, although this notation for the families of tiles is not unique, it is quite convenient for our purposes because of its analogy with the winding numbers of PO's.

Let us next discuss how the homoclinic tangle obtained for $\theta_i=90°$ can be used to predict and understand the dynamics of the He-Cu collisions for other angles of incidence. For $\theta_i\neq 90°$ the partition of the energy between the two modes will be different from that of the PUPO. However, it is obvious that the initial conditions of Eq. (2) also generate a manifold in phase space, which can be plot on top of the homoclinic tangle for $\theta_i=90°$ [see Fig. 3(c)]. If the manifold is such that it does not intersect the stable branch of the homoclinic tangle, it will evolve close to the unstable branch without ever entering the interaction region [the thick line in Fig. 3(c)], and the scattering will be regular. On the other hand, if a portion of it intersects the stable branch, that portion will fall at some point into the entrance lobe of the turnstile, leading to temporary trapping. Moreover the manifold originated by the initial conditions will not cross all the tiles within the intersected lobe of the stable branch (some of the inner ones will be missed), therefore the central part of the chattering region in the θ_f-b plots will be different than that at $\theta_i=90°$, but the lobes intersected will display the same pattern in the θ_f-b plot because they follow the same tiling as the PUPO does. The corresponding invariant pattern will be the same as that of the chattering region of Fig. 1. This explains the invariance of the scaling laws and other fractal features with respect to the incident angle.

IV. PERIODIC ORBITS IN THE INTERACTION REGION

In this section we will investigate in further detail the dynamical structure of the interaction region, especially in relation to PO's. In our system we have a special type of PO. Since the potential-energy surface extends to infinity in the

x coordinate and our system is open, the trajectories are mainly unbounded. However, due to the periodicity of the potential we have some trajectories which are confined in z, executing a periodic motion along x. Due to the way in which our SOS is calculated, these trajectories will cross it only in a finite number of points visiting them periodically: they are the equivalent to the usual PO's of the more familiar bounded systems.

Periodic orbits form a dense set in phase space. Although it is not possible to locate all of them, a general view of the evolution of the main families of PO's with some parameter, usually the energy, provides valuable information of the dominant classical dynamical features. The main families of PO's are usually defined from Weinstein's theorem [25], which states that around any equilibrium point of the potential a number of PO's equal to the number of degrees of freedom of the system emerges. Multishooting and relaxation numerical methods have been applied to propagate the main families and find bifurcations for systems up to six degrees of freedom [26] in a rather systematic way. However, this procedure is very time consuming since for every energy step we can locate only one PO. For Hamiltonian systems with some type of symmetry, PO's having that symmetry can be more easily generated in a very systematic way by using the method of the propagation of the symmetry lines. The essence of the method [27] consists of finding for each energy the intersections of a symmetry line with its successive iterations under the Poincaré map.

The dominant symmetry lines can be located by finding the set of points left invariant under the composition of a reflection σ_x and time reversal T operators [27] acting on a phase space point $\mathbf{q}=(x_0+\epsilon,z,P_x,P_z)$ as

$$\sigma_x\mathbf{q}=(x_0-\epsilon,z,-P_x,P_z) \tag{3}$$

and

$$T\mathbf{q}=(x_0+\epsilon,z,-P_x,-P_z). \tag{4}$$

This set of points exists in our model only for the Cu(110) potential, and is given by the line

$$S_0=(x_0,z,P_x,0), \tag{5}$$

where $x_0=0,a$ or $x_0=a/2$. Denoting by P the Poincaré map as defined at the beginning of Sec. III and by P^n its nth iteration, it can be shown [27(a)] that the points given by the intersections

$$P^n\circ S_0\cap S_0 \tag{6}$$

are periodic orbits of period $2n$ and divisors.

To obtain the PO's of an even period, we have to define in addition the symmetry line S_1 made of points left invariant under $P\circ S_0$ which is precisely the set of points $P^{1/2}\circ S_0$, i.e., one of the two dominant symmetry lines evolved one-half of the Poincaré map. Again intersections

$$P^n\circ S_1\cap S_0 \tag{7}$$

will be PO's of period $2n+1$ and divisors. In this way we can generate all primitive families of symmetric PO's of different periods.

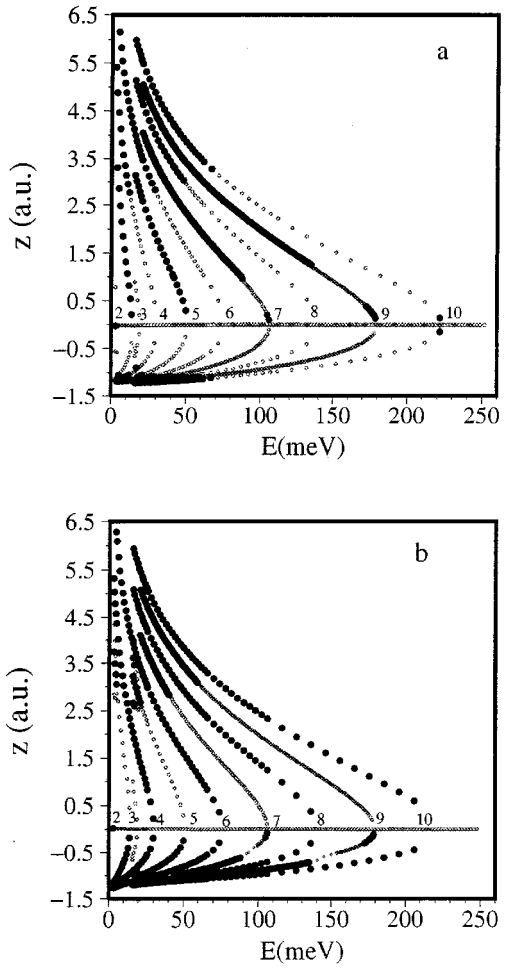

FIG. 4. Periodic orbit bifurcation diagram corresponding to the He-Cu(110) scattering obtained by propagation of the (a) $x_0=a$, and (b) $x_0=a/2$ symmetry lines. Full circles correspond to unstable periodic orbits, while the stable ones have been represented by empty circles.

The bifurcation diagrams constructed using this procedure are shown in Fig. 4. We only followed up to the fifth iteration of the symmetry lines S_0 and S_1. Some representative examples of these PO's are shown in Fig. 5. Two points are worth discussing in relation to Fig. 4. In the first place, we find in both plots a central period-1 PO (CPO), which is common to both symmetry lines and constitutes the main family, thus originating the other higher period PO's through bifurcations. The second point is that, contrary to what usually happens in bounded generic Hamiltonian systems, the behavior is less chaotic, in the sense that unstable PO's with higher periods disappear, as energy increases. This is seen in Fig. 6, where the homoclinic tangle corresponding to $E=400$ meV is represented. Only the stable CPO seems to survive with a big structure of regular *KAM* islands around it, but still some chaos exist due to very high-period unstable PO's, although is not visible in the scale of the figure. The CPO remains stable until very small energies (approximately 4 meV), when it becomes unstable due to a period-doubling bifurcation.

The method of propagating symmetry lines allows the localization of PO's, but cannot predict which ones will appear at a given energy. The occurrence of bifurcations giving rise

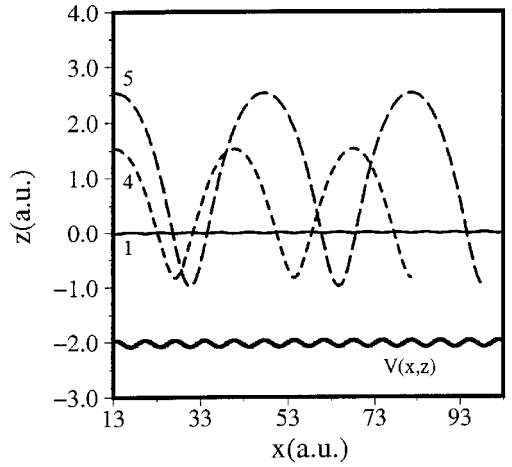

FIG. 5. Periodic orbits of periods 1 (CPO), 4, and 5 for the He-Cu(110) scattering at $E=21$ meV. The equipotential contour line has also been included.

to PO's can be predicted using Hamiltonian bifurcation theory [28]. This theory indicates that in two-dimensional systems only five classes of bifurcations can take place: saddle center or pitchfork, period doubling, touch and go, four-island chain, and m-island chain (see Ref. [28(c)] for a detailed account).

The location of each new bifurcation of period m can be found considering the trace of the Jacobian matrix,

$$\mathbf{J}_m=\begin{pmatrix} \partial P_z^m/\partial P_z^0 & \partial P_z^m/\partial z^0 \\ \partial z^m/\partial P_z^0 & \partial z^m/\partial z^0 \end{pmatrix}, \tag{8}$$

where z^0 and P_z^0 are the initial values of z and P_z in the SOS, and z^m and P_z^m their values after the mth iteration of the Poincaré map. According to bifurcation theory at the bifurcation points the trace of this Jacobian equals two. Moreover, this trace can be related to that of the Jacobian for the CPO (period-1 PO), so that an m bifurcation occurs when

$$\mathrm{Tr}(\mathbf{J}_1)=2\cos(2\pi j/m), \tag{9}$$

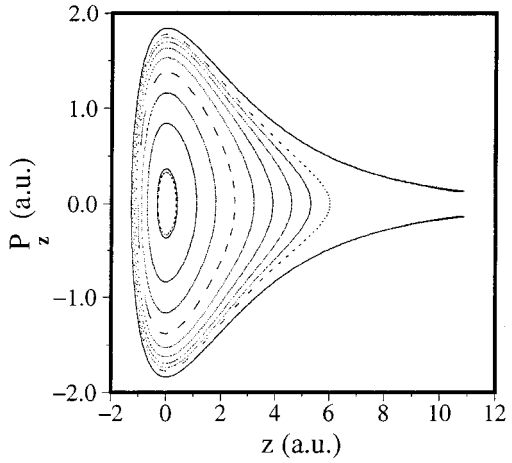

FIG. 6. Homoclinic tangle corresponding to the He-Cu(110) scattering system at $E=400$ meV.

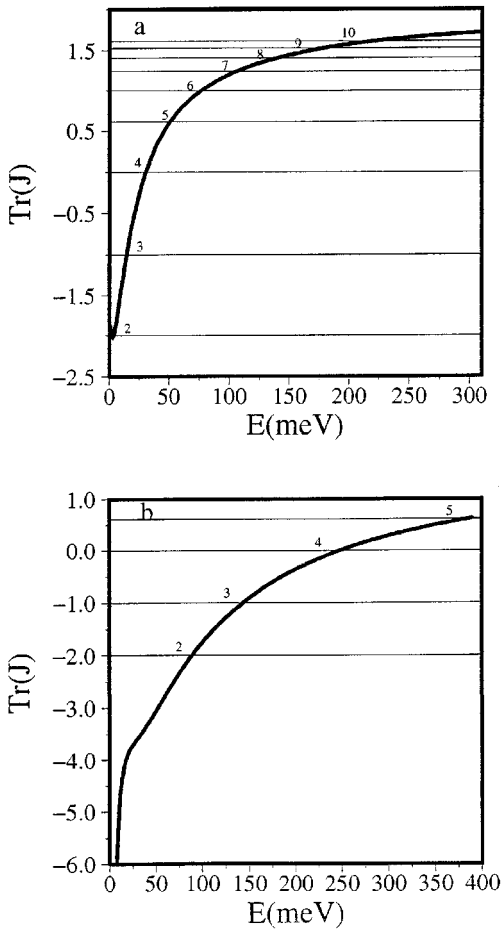

FIG. 7. Trace of the central periodic orbit (CPO) Jacobian matrix for the scattering off (a) Cu(110) and (b) Cu(117) surfaces.

with $j=1$ if $m\leqslant 4$, $j=1$ and 2 if $m=5$, and so on. In this way it is possible to predict *locally* the sequence of bifurcations of any given PO. It should be emphasized, however, that there is no general global theory that accounts for all possible bifurcations of a given PO. A notable exception is the theory developed for the Hénon map by Tsuchiya and Jaffé based on the symbolic dynamics of permutation groups [29].

In Fig. 7(a) the CPO Jacobian matrix trace as a function of the energy is represented. The bifurcations predicted by Eq. (9) and observed in Fig. 4 have also been marked in the figure. Note that according to Eq. (9) an accumulation of bifurcations of increasingly higher period is expected as we approach the original saddle-center bifurcation. For many chaotic scattering systems the generic route for the onset of chaos has been described to be the appearance of a saddle-center bifurcation creating one stable PO and one unstable PO (the CPO and the PUPO in our case) [9,10(e)], with the homoclinic oscillations giving rise to complex formation. Our model system has the peculiarity that the trace of the CPO tends asymptotically to the point of that bifurcation as the energy increases; that is, we always have some region of chaos. In fact, the PUPO has $\mathrm{Tr}(\mathbf{J}_1)=2$ (it is a parabolic orbit). Obviously, this is a problem of our model potential, since at high energies only direct scattering is expected to be observed experimentally. On the other side of the bifurcation diagram the CPO remains stable to very low energies,

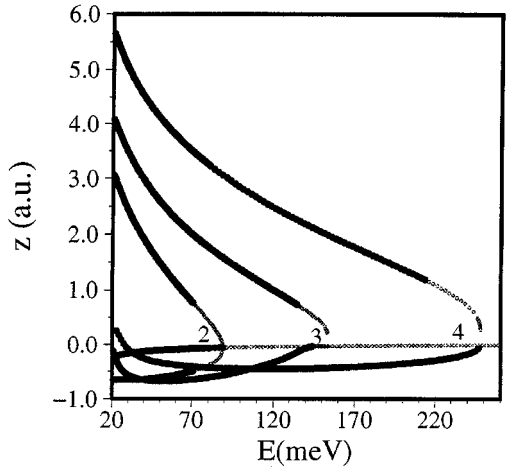

FIG. 8. Periodic orbit bifurcation diagram corresponding to the He-Cu(117) scattering.

where it becomes unstable due to a period-doubling bifurcation.

We will end this section with some comments about the dynamics for the Cu(117) surface. In this case the potential has no reflection symmetry, and therefore it is not possible to use the method of symmetry line propagation to construct bifurcation diagrams. However, it is still possible to obtain some valuable information from the Hamiltonian bifurcation theory. The CPO was calculated and happens to be very similar to that for Cu(110), although without showing the same symmetry. The trace of the Jacobian, as a function of the energy, is shown in Fig. 7(b); in it the locations of the main bifurcations have been indicated. This PO turns unstable at $E \simeq 89$ meV due to a period-doubling bifurcation, after which the system becomes hyperbolic [remember the homoclinic tangle in Fig. 2(b)]. Also, Fig. 7(b) shows that the Lyapunov exponent decreases without limit as E decreases, and tends to infinite at ($E \leqslant 4$ meV); this explains the rapid transport between the scattering and the interaction regions described in Sec. III. Despite its lack of symmetry, the Cu(117) potential presents the same structure of primitive families of PO's than that of Cu(110). The bifurcation diagrams containing the first families are shown in Fig. 8. We have included only PO's up to period 5. Continuation of PO's of higher periods at low energies presents numerical problems due to their high instabilities. The PO's were located giving as initial conditions specific homoclinic points of the PUPO, as will be explained in Sec. VI, and continued in energy using a shooting method.

V. PERIODIC AND HOMOCLINIC ORBIT STRUCTURES THROUGH SYMBOLIC DYNAMICS

Although the number of trajectories in the chattering region is uncountable, all of them belonging to the same pair of icicles (those labeled with the same chain of numbers but different signs [12(a)]) correspond to the same kind of trapped trajectories, and therefore can be associated with the same type of homoclinic orbits. The purpose of the present section is to provide a connection between the homoclinic orbits (and consequently the different kinds of chaotic trajectories) and the PO's in the interaction region. It is known that

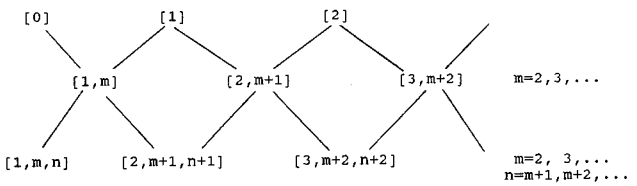

FIG. 9. Construction tree for the first three generations of homoclinic orbits in the He-Cu(110) scattering at $E = 21$ meV.

close to a homoclinic point there is an infinite sequence of PO's [30] with increasing period. This fact is based on the existence of a Birkhoff normal form convergent around the stable and unstable manifolds of an unstable fixed point of the Poincaré map. Indeed, unstable PO's have been calculated analytically using the Birkhoff normal form for quadratic maps. In our case the correspondence between the homoclinic points and PO's arises naturally if we consider that each homoclinic point of the PUPO corresponds to a certain chaotic trajectory, and there can be a PO of similar topology associated with it. In order to envisage this relation, let us consider simple symbolic schemes for homoclinic orbits and PO's.

Following the same labeling scheme used in Sec. II to classify the icicles of the chattering region, a symbolic tree for the organization of homoclinic orbits can be generated. The result is shown in Fig. 9. Here the symbolic chains have the same meaning as for the icicles, except for the fact that the signs have now been dropped since we are not interested in distinguishing between the left and right parts of the fractal for homoclinic orbits. Each orbit in the ith generation (making i bounces against the surface) is labeled by i integers. The first one gives the number of unit cells jumped in the first bounce, the second the number of unit cells jumped jointly in the first and second bounce, and so on. Notice that, in each generation, the variation of the indices is related. For instance, in the third generation for each m the last index n is made to vary from $m+1$ to infinity (producing the whole series of homoclinic orbits inside the same gap of the fractal). Notice also that the order in which these sequences of homoclinic orbits appear in the θ_f-b plots is preserved.

Now we can take a further step in our classification procedure, and assign to each different homoclinic orbit a ''winding number,'' p/q, such that p is the number of symbols of the labeling chain, and q is the last number in that chain. Let us remark that p gives the total number of outer turning points, or oscillations in the z coordinate, and q the total number of unit cells traveled, or oscillations in the x coordinate; therefore p/q has the physical meaning of a winding number.

Considering now the PO's of the system, any given PO can be assigned also to a winding number p/q, with the same meaning as above. In Sec. IV we obtained, for instance, PO's with winding numbers 1/1 to 1/10 (Fig. 4) for Cu(110). It was demonstrated that for two-dimensional area-preserving maps, the end points of resonance intervals can be organized according to a Farey tree scheme [31–33]. The Farey tree, which is equivalent to the continued fraction expansion of the irrationals, organizes the rationals in sequences of best convergents to a given rational or irrational number. This tree can be generated starting from the end points of the unit

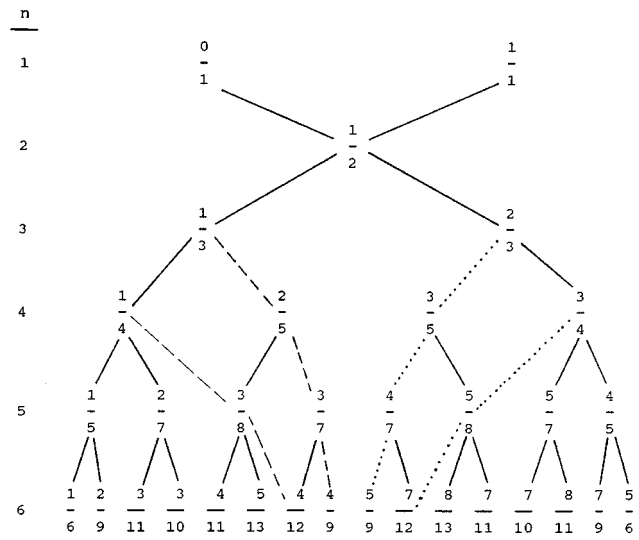

FIG. 10. Farey tree organization of the rational numbers. The integer n indicates the number of the generation. The two first sequences converging to $\frac{1}{2}$ from the ''left'' and from the ''right'' have been indicated with dashed and dotted lines respectively.

interval, written as 0/1 and 1/1, and calculating the Farey mediants between two *neighbor* rationals p/q and r/s as $(p+r)/(q+s)$. The resulting tree is shown in Fig. 10. It is well known [33] that sequences converging to different rational or irrational numbers are similar to each other, and therefore there are scaling laws implicit in the Farey tree structure relating for instance the positions of resonance intervals. The scaling laws present in the Farey tree provide an explanation of the scaling laws that we observe in the fractal chattering region of the θ_f-b plots. This can be seen if we consider that sequences of convergents to a given rational of the form $1/j$ $(j=1,2,\ldots)$ can be constructed according to the following rule:

$$\frac{1}{j+\dfrac{m}{n}}, \tag{10}$$

where n varies from 1 to infinity as we pass from one generation to the next along the Farey tree, and $m=1$ corresponds to the first sequence, $m=2$ to the second sequence, etc. Notice that the sequence corresponding to $m=1$ generates the best approximation, which is precisely the Farey sequence. For example, for $j=2$, the sequences approximating 1/2 are: $\frac{1}{3},\frac{2}{5},\frac{3}{7},\frac{4}{9},\ldots$ for $m=1$; $\frac{1}{4},\frac{2}{6},\frac{3}{8},\frac{4}{10},\ldots$ for $m=2$, etc. The first two sequences were represented with a dashed line in Fig. 10.

All the previous discussions assume convergence to a given rational $1/j$ from the ''left'' of the Farey tree, but we can also converge to the same numbers from the ''right.'' In this case the rule is

$$\frac{1}{j-\dfrac{m}{n+m}}, \tag{11}$$

with m and n having the same meaning as in Eq. (10). The first two sequences ($m=1$ and 2) converging to 1/2 are represented with dotted lines in Fig. 10.

Let us now analyze how chains of symbols corresponding to homoclinic orbits can be organized in sequences of convergents similar to those of the Farey tree. First of all, notice that inside a given gap or interval all homoclinic orbits are obtained, fixing all symbols in the chain except the last one, which is increased by one each time. Therefore this sequence converges always to 0/1, the initial point of the interval in Fig. 10. This defines the intragenerational scaling parameter α. As we numerically observed [12(c)], it does not matter in which generation or gap of the θ_f-b plot you are; the positions of the icicles always scale with α as one goes to the edges of the interval.

To see how the intergenerational self-similarity is achieved, we have to consider sequences of homoclinic orbits in consecutive generations, occupying the same relative positions with respect to the *parents*. For instance, take the interval between orbits [2] and [3]; the *daughters* between them are given by the series [3,4],[3,5],[3,6], ... (see Fig. 9). The *daughter* occupying the second place, [3,5], corresponds to a winding number 2/5. Taking now the *daughters* between this and [3,4], the new series is now [3,5,6],[3,5,7], ..., whose second element has a winding number of 3/7. Repeating this procedure we obtain the sequence: 1/3,2/5,3/7,4/9, ..., which is precisely the Farey sequence convergent to 1/2 from the ''left,'' i.e., Eq. (10) above with $j=2$ and $m=1$. If we take the interval between orbits [3] and [4], and repeat the procedure for the second elements of successive generations, the sequence 1/4,2/6,3/8,4/10, ... is obtained, which is the sequence converging to 1/2 with $m=2$ following Eq. (10). If we look at other relative positions different from the second, the same scheme is valid, but now the convergence is to $1/j$, being j the relative position. One can show that the whole symbolic tree for homoclinic orbits follows the same organization as the Farey tree for PO's, if we look at sequences of convergents to a given rational $1/j$. The correspondence is made explicit by the following rules:

(1) For a given homoclinic orbit $[l,m,n,\ldots,r]$, the sequences of daughters of the form $[l,m,\ldots,r,r+j]$, $[l,m,\ldots,r,r+j,r+2j]$, ..., $[l,m,\ldots,r,r+j,\ldots,r+kj]$ correspond to a sequence of convergents to the number $1/j$. These orbits occupy the same relative position inside a given interval.

(2) If $l=j+1$ (being l the first number of the chain) we have the Farey sequence from the ''left,'' Eq. (10) above with $m=1$. If $l=j-1$ we have the Farey sequence from the ''right,'' Eq. (11) with $m=1$.

(3) In general, $l-j=m$, m being the number of the sequence convergent to $1/j$ in the equations above. If $m>0$, we converge from the ''left,'' Eq. (10), following sequence m. If $m<0$ we converge from the ''right,'' Eq. (11), following sequence $|m|$. Notice that for $m=0$ we simply obtain a sequence of the form n/nj in both equations, i.e., the sequence is just a multiple of $1/j$ and one can see that the homoclinic orbits are a pruning of the corresponding PO (those jumping the same number of unit cells between all the bounces).

This correspondence means in turn that we have many different intragenerational scaling laws if we are close to the center of the fractal: one for the convergence to 1/1, a different one for the convergence to 1/2, etc. But, since we are interested in the asymptotic self-similar part of the fractal [12(c)], the asymptotic intragenerational scaling law β is calculated for convergence to $1/j$ when j tends to infinity. Also one can think that different sequences of convergents to a given rational $1/j$ [the sequences $m=1,2,\ldots$ in Eqs. (10) and (11)] have different scaling laws; however, they are redundant. The denominators of these sequences always grow *harmonically*, the only difference being that they are ''shifted'' to the center of the Farey tree by $m-1$ steps before going down to the next generation (see the dashed and dotted lines in Fig. 10). This can explain the fact that if we consider an intergenerational scaling factor β_i as the factor necessary to scale a given gap or icicle of one generation into the gap of the *next* generation differing by i *relative* positions, we would have

$$\beta_i=\alpha^i\beta. \tag{12}$$

Recall that β is the intergenerational scaling factor that scales icicles or gaps of different generation with the *same* relative position. If a Cantor set for the singularities in the θ_f-b plots (Fig. 1) is constructed by removing in each step the icicles corresponding to the same generation, at the nth step the dimension δ_n of the set is implicitly defined by [34]

$$\sum_i G_i^{D_n}=1, \tag{13}$$

where G_i are the widths of the gaps between the icicles of the nth generation, and the sum runs over all of the gaps. Making use of the fact that, in the same way as the icicles, the widths of the gaps scale as α inside the same generation and as β from one generation to the next, and of Eq. (12), one can arrive at the following expression for the fractal dimension taking the limit $n\to\infty$ [11(a)]:

$$\alpha^D+2\beta^D=1. \tag{14}$$

This equation was used to calculate the intergenerational scaling law β once the fractal dimension of the set is known.

In order to see the correspondence of the scaling for PO's and homoclinic orbits, we plot in Fig. 11 a sequence of five tiles for the He-Cu(110) scattering that can be denoted (1:8),(1:9), . . . ,(1:12) and the corresponding fixed points of the symmetric PO's with winding numbers 1/8,1/9, . . . ,1/12. From the figure it is clear that asymptotically the homoclinic orbit (corner of the tile) tends to the corresponding PO. It is reasonable to think that, once a scattering trajectory enters the interaction region, if it gets close to the stable manifold of a particular unstable PO it will remain close to it during some time. If we scale the positions of the PO's of the form $1/j$ along the symmetry lines according to the relation

$$\delta_k=\frac{z_{k+1}-z_k}{z_k-z_{k-1}}, \tag{15}$$

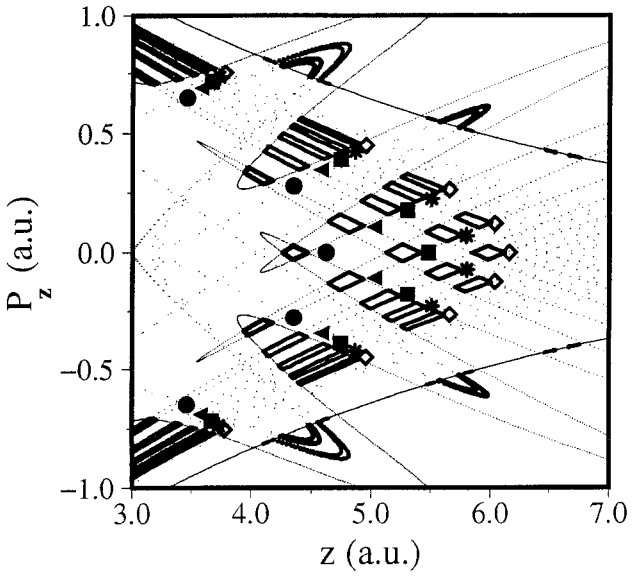

FIG. 11. Enlargement of the interaction region of the homoclinic tangle for the He-Cu(110) scattering at $E=21$ meV shown in Fig. 3. Five families of tiles from (1:8) to (1:12) (thick lines) are shown together with the associated periodic orbits with winding numbers from $\frac{1}{8}$ to $\frac{1}{12}$ (circles, triangles, squares, asterisks, and diamonds, respectively).

where z_k is the position of the kth PO in the corresponding symmetry line, a value of $\delta_k=0.98$ is obtained for $k\to\infty$ at a fixed scattering energy of 21 meV. In practice we had to go up to $k=56$ to achieved convergence in the second decimal figure. If we scale in the same way the positions of the extremes of the icicles in the corresponding θ_f-b plot we obtain the same value $\alpha=0.98$, which is precisely the intragenerational scaling law. In this case the convergence to the final asymptotic value is slower than for δ_k (we needed to go up to icicles $[130^{\pm}]$ for the same convergence), but the final result is identical inside the numerical precision.

Finally, let us point out that the symbolic tree shown in Fig. 10 is valid for hyperbolic dynamics, when PO's of all periods, $1/j$ starting with $j=1$, are accessible for the scattering trajectories (since the CPO has turned unstable). This is the case for the scattering off Cu(117) surfaces at $E=21$ meV. For the Cu(110) surface at the same energy (nonhyperbolic dynamics) the symbolic tree for homoclinic orbits starts in this case from $j=8$, and PO's of lower periods are not accessible to the scattering trajectories. The Farey tree will then be truncated, but the same relations than for the hyperbolic case *hold*.

VI. CONCLUSIONS

The scattering of ^{4}He atoms from corrugated Cu surfaces is known to be classically irregular or chaotic [12]. This can be seen for example in the deflection angle vs impact parameter plots, where ill-behaved regions of fractal nature appear for certain initial conditions. These chattering regions consist of smooth subdomains, which repeat on all scales. Moreover, this structure can be related to the topology of the corresponding classical trajectories [12(a),12(b)].

In this paper we have shown that the fractal character of these scattering function plots can be very well understood

when analyzed in phase space. In order to do that we have defined suitable Poincaré surfaces of section, taking advantage of the fact that the potential of our system is periodic. The tiling pattern imposed in phase space by the homoclinic tangle of one principal unstable PO (PUPO), corresponding to a motion of the He atom parallel to the surface in the asymptotic region, is clearly determinant of all features of the corresponding scattering dynamics. The main characteristics of the fractal region (invariance with respect to angle of incidence of the He particles, labeling scheme of the icicles) have been explained by investigating in detail the existing phase-space structures. Also, the main families of symmetric PO's have been obtained as a sequence of higher-order period bifurcations from a principal stable period-1 PO (CPO). This PO is the stable companion of the PUPO, which generates the fractal tiling. While the homoclinic tangle of this last orbit governs the behavior of the chaotic scattering trajectories, the main features inside the interaction region (a *KAM* island structure, and hyperbolic and nonhyperbolic regimes) seem to be determined by the sequence of bifurcations of the CPO. We have demonstrated, using a simple symbolic code for generating the sequences of homoclinic orbits, that a very close correspondence exists between the organization of homoclinic scattering trajectories and the Farey tree organization known for periodic orbits. This correspondence also explains the existence of the asymptotic self-similarity and scaling laws present in the chattering region of all chaotic scattering problem.

Finally, let us mention that this explicit correspondence can be exploited to locate periodic orbits of a desired winding number. As we know that, close to a homoclinic orbit whose winding number is a rational of the Farey tree, a periodic orbit of the same winding number must exist, we simply use the position of the homoclinic orbit, known from the θ_f-b plot, as an initial guess in an appropiate Poincaré SOS using for instance a multishooting method for convergence. However, we found in practice that only PO's of low rational winding numbers are easily located since in general high winding numbers are very unstable.

ACKNOWLEDGMENTS

Very useful discussions with Professor C. Jaffé and Dr. A. A. Zembekov are gratefully acknowledged. This work was supported in part by DGES (Spain) under Contract Nos. PB95-71 and PB95-425. R.G. gratefully acknowledges financial support from the Ministerio de Educación y Ciencia (Spain).

[1] M. Alagia, N. Balucani, L. Cartechini, P. Casavecchia, E. H. van Kleef, G. G. Volpi, F. J. Aoiz, L. Bañares, D. W. Schwenke, T. C. Allison, S. L. Mielke, and G. G. Truhlar, Science **273**, 1519 (1996).

[2] J. D. McClure, J. Chem. Phys. **51**, 1687 (1969); **52**, 2712 (1970); **57**, 2810 (1972); **57**, 2823 (1972); D. S. Sholl and R. T. Skodje, Phys. Rev. Lett. **75**, 3158 (1995).

[3] B. Eckhardt, Physica D **33**, 89 (1988); U. Smilanski, in *Chaos and Quantum Physics*, edited by M.-J. Giannoni, A. Voros, and J. Zinn-Justin (Elsevier, Amsterdam, 1992), p. 371.

[4] C. Jung, J. Phys. A **19**, 1345 (1986); **20**, 1719 (1987).

[5] M. J. Davis, J. Chem. Phys. **83**, 1016 (1985); M. J. Davis and S. K. Gray, *ibid.* **84**, 5389 (1986); G. P. Brivio and Z. W. Gortel, Surf. Sci. **261**, 359 (1992); G. P. Brivio and M. Torri, Phys. Rev. B **48**, 4835 (1993); G. P. Brivio, M. L. Rossi, M. Torri, and Z. W. Gortel, Phys. Rev. Lett. **76**, 3376 (1996).

[6] R. A. Marcus, J. Chem. Phys. **54**, 3965 (1971); **57**, 4903 (1972); W. H. Miller, Adv. Chem. Phys. **25**, 69 (1974); **30**, 77 (1975).

[7] C. C. Rankin and W. H. Miller, J. Chem. Phys. **55**, 3150 (1971).

[8] N. Hill and V. Celli, Surf. Sci. **75**, 577 (1978).

[9] S. Bleher, C. Grebogi, and E. Ott, Physica D **46**, 87 (1990); M. Ding, C. Grebogi, E. Ott, and J. Yorke, Phys. Rev. A **42**, 7025 (1990); R. Blümel and U. Smilanski, Physica D **36**, 111 (1989); G. Troll and U. Smilanski, *ibid.* **35**, 34 (1989); J. Phys. A **20**, 5971 (1987); C. Jung and H. J. Scholz, *ibid.* **20**, 3607 (1987).

[10] (a) L. Gottdiener, Mol. Phys. **29**, 1585 (1975); (b) N. Agmon, J. Chem. Phys. **76**, 1309 (1982); (c) D. W. Noid, S. K. Gray, and S. A. Rice, *ibid.* **84**, 2649 (1986); (d) J. C. Polanyi and R. J. Wolf, Ber. Bunsenges. Phys. Chem. **86**, 356 (1982); (e) I. Burghardt and P. Gaspard, J. Phys. Chem. **99**, 2732 (1995).

[11] (a) A. Tiyapan and C. Jaffé, J. Phys. Chem. **99**, 2765 (1993); (b) **101**, 10 393 (1994); (c) **103**, 5499 (1995).

[12] (a) F. Borondo, C. Jaffé, and S. Miret-Artés, Surf. Sci. **317**, 211 (1994); (b) R. Guantes, F. Borondo, C. Jaffé, and S. Miret-Artés, Int. J. Quantum Chem. **52**, 515 (1994); (c) R. Guantes, F. Borondo, C. Jaffé, and S. Miret-Artés, Phys. Rev. B **53**, 14 117 (1996).

[13] J. M. Petit and M. Hénon, Icarus **66**, 536 (1986); B. Eckhardt and H. Aref, Philos. Trans. R. Soc. London, Ser. A **326**, 655 (1988).

[14] C. Lipp and C. Jung, J. Phys. A **28**, 6887 (1995); B. Rückerl and C. Jung, *ibid.* **27**, 6741 (1994).

[15] (a) Z. Kovács and L. Wiesenfeld, Phys. Rev. E **51**, 5476 (1995); (b) H. Wadi and L. Wiesenfeld, *ibid.* **55**, 271 (1997).

[16] K. T. Hansen and A. Kohler, Phys. Rev. E **54**, 6214 (1996).

[17] D. Gorse, B. Salanon, F. Fabre, A. Kara, J. Perreau, G. Armand, and J. Lapujoulade, Surf. Sci. **47**, 611 (1984).

[18] B. B. Mandelbrot, *The Fractal Geometry of Nature* (Freeman, New York, 1983).

[19] S. Wiggins, *Introduction to Applied Non Linear Dynamical Systems and Chaos* (Springer, New York, 1990).

[20] (a) Y.-C. Lai, M. Ding, C. Grebogi, and R. Blümel, Phys. Rev. A **46**, 4661 (1992); (b) C. F. Hillermeier, R. Blümel, and U. Smilansky, *ibid.* **45**, 3486 (1992); (c) C. F. F. Karney, Physica D **8**, 360 (1983); (d) J. D. Meiss and E. Ott, *ibid.* **20**, 387 (1986).

[21] S. Benkadda, Y. Elskens, B. Ragot, and J. T. Mendonca, Phys. Rev. Lett. **72**, 2859 (1994).

[22] R. Guantes and F. Borondo (unpublished).

[23] R. S. MacKay, J. D. Meiss, and I. C. Percival, Physica D **13**, 55 (1984); **27**, 1 (1987); D. Bensimon and L. D. Kadanoff, *ibid.* **13**, 82 (1984).

[24] T. Horita, H. Hata, R. Ishizaki, and H. Mori, Prog. Theor. Phys. **83**, 1065 (1990); M. A. Sepulveda, R. Badii, and E. Pollak, Phys. Rev. Lett. **63**, 1226 (1989).
[25] A. Weinstein, Invent. Math. **20**, 47 (1973); J. Moser, Commun. Pure Appl. Math. **29**, 727 (1976).
[26] R. Prosmiti and S. C. Farantos, J. Chem. Phys. **103**, 3299 (1995).
[27] (a) R. DeVogelare, in *Contributions to the Theory of Non Linear Oscillations*, edited by S. Lefschetz (Princeton University Press, Princeton, 1958), Vol. IV, p. 53; (b) J. Heagy and J. M. Yuan, Phys. Rev. A **41**, 571 (1990); (c) C. Jung and P. H. Richter, Phys. Rev. A **23**, 2847 (1990).
[28] (a) K. R. Meyer, Trans. Am. Math. Soc. **149**, 95 (1970); (b) M. A. M. de Aguiar, C. P. Malta, M. Baranger, and K. T. R. Davies, Ann. Phys. (N.Y.) **180**, 167 (1987); (c) J.-M. Mao and J. B. Delos, Phys. Rev. A **45**, 1746 (1992).
[29] M. Tsuchiya, Ph.D. Thesis, West Virginia University, 1995.
[30] G. L. da Silva Ritter, A. M. Ozorio de Almeida, and R. Douady, Physica D **29**, 181 (1987).
[31] R. S. MacKay, in *Physics of Particle Accelerators*, AIP Conf. Proc. No. 153 (AIP, New York, 1987).
[32] A. A. Zembekov, Phys. Rev. A **42**, 7163 (1990); P. Veerman, Physica D **29**, 191 (1987).
[33] P. Cvitanovic, B. Shraiman, and B. Söderberg, Phys. Scr. **32**, 263 (1985).
[34] See, for example, T. Vicsek, *Fractal Growth Phenomena* (World Scientific, Singapore, 1992), pp. 20 and 21.